

Thermal Monitoring

BY VICTOR PIKOV
AND PETER H. SIEGEL

Raman Spectrometer System for Remote Measurement of Cellular Temperature on a Microscopic Scale

A simple setup is demonstrated for remote temperature monitoring of water, water-based media, and cells on a microscopic scale. The technique relies on recording changes in the shape of a stretching band of the hydroxyl group in liquid water at $3,100\text{--}3,700\text{ cm}^{-1}$. Rather than direct measurements in the near-infrared (IR), a simple Raman spectrometer setup is realized. The measured Raman shifts are observed at near optical wavelengths using an inverted microscope with standard objectives in contrast to costly near-IR elements. This allows for simultaneous visible inspection through the same optical path. An inexpensive 671-nm diode pump laser ($<100\text{ mW}$), standard dichroic and low-pass filters, and a commercial 600–1,000 nm spectrometer complete the instrument. Temperature changes of 1°C are readily distinguished over a range consistent with cellular processes ($25\text{--}45^\circ\text{C}$) using integration times below 10 s. Greatly improved sensitivity was obtained by an automated two-peak fitting procedure. When combined with an optical camera, the instrument can be used to monitor changes in cell behavior as a function of temperature without the need for invasive probing. The instrument is very simple to realize, inexpensive compared with traditional Raman spectrometers and IR microscopes, and applicable to a wide range of problems in microthermometry of biological systems. In a first application of its kind, the instrument was used to successfully determine the temperature rise of a cluster of H1299 derived human lung cells adhered to polystyrene and immersed in phosphate-buffered saline (PBS) under exposure of RF millimeter wave radiation (60 GHz , 1.3 , 2.6 , and 5.2 mW/mm^2).



© PHOTODISC

Raman Spectroscopic Measurements

The remote measurement of temperature on a microscopic scale has been enabled by the advent of the IR microscope [1]. However, this instrument is extremely costly (e.g., Thermo Scientific Nicolet iN10 IR microscope is currently priced at US\$75,000–100,000), and when used for biological measurements, where specimens are often sandwiched between plastic or glass plates or immersed in liquids, the accuracy suffers from differences in emissivity in the various layers that must be penetrated before reaching the sample. It is also difficult to discern the temperature emanating specifically from a cellular or tissue layer immersed in culture medium since water is a very strong IR absorber. Consequently, only the surface temperature has been accurately determined by this type of system. A novel method for remote probing the temperature of liquid water on a

Digital Object Identifier 10.1109/EMEB.2009.935468

microscopic scale was demonstrated recently [2], [3]. This technique uses the spectroscopic measurement of the near-IR stretching band of water [4], which changes both its absorption amplitude and shape as a function of temperature. The focus of the IR studies was the change in absorption amplitude with temperature using a sample with controlled thickness. Similar to water, the spectral absorption and reflection signatures of assorted biological solutions and tissues exhibited a gradual change with temperature in the near-IR water lines of 960, 1,200, and 1,400 nm [5]. In both studies [4], [5], regression analyses were performed, and the derived linear models were able to accurately predict the measured temperature change in the tissue for a given variation in spectral absorbance. In the wavenumber range between 3,100 and 3,700 cm^{-1} (wavelengths from 2.7 to 3.2 μm), the broad Raman band is due to intramolecular vibrational motion of the hydroxyl group of water. Possible vibrational modes include symmetric stretching (ν_1), an overtone of bending ($2\nu_2$), and antisymmetric stretching (ν_3) [6], but experimental studies indicate that only the ν_1 mode is prominent in the Raman measurements [7], [8]. The width and multippeak shape of the ν_1 mode has been attributed to coupling of the hydroxyl group stretching with the energy of intra- and intermolecular hydrogen bonds [6], [9]–[11]. Formation of these hydrogen bonds can reduce the wavenumber [7] and amplitude [12] of this hydroxyl stretching motion. The band profile has been decomposed into several Gaussian components,

possibly indicating the varying number of hydrogen bonds [6] or their strength (weak versus strong) [11]. Different authors identified two [13], three [11], [14], four [6], [15], or even five components [16] in the hydroxyl stretching band, whereas a recent rigorous analysis of assorted decomposition approaches [17] indicated that a two-component decomposition is adequate for liquid water at temperatures ranging from 5 to 100 $^{\circ}\text{C}$.

This spectral signature of water, although very distinct, falls well into the near-IR region, making direct observation through a typical optical system very difficult. However, by employing well-established Raman spectroscopy techniques, it is possible to shift the measured spectrum to the near-visible region of 800–900 nm, which permits the use of standard microscope objectives and filters while avoiding the background biofluorescence of the visible spectral region. In this article, we present a very simple instrument arrangement for observing the 3,200–3,700 cm^{-1} hydroxyl stretching band and show that an accurate estimation of temperature on a microscopic scale can be obtained with short detection time and low-pump, laser-power level, making it compatible with studies of living cells and tissues. In addition, we show that a narrow spectral signature from polystyrene, a common culture dish material, is located near the hydroxyl stretching band and can be used to determine the axial focal plane within the culture dish containing the cells. The method can be used to accurately monitor the temperature of biological specimens in plastic or quartz (but not glass) containers with minimal cost and great flexibility. Both the instrumentation and initial measurements in biological samples are presented.

Growing interest in the effects of millimeter and submillimeter wave radiation on biological systems, especially cells and cellular processes, prompted the first application for the Raman spectrometer in monitoring and calibrating the temperature rise of living cells exposed to strong RF fields. The results of the first experiments performed on direct microscopic observations of the impact of 60-GHz radiation on the temperature of H1299 human-derived lung cells adhered to a polystyrene membrane and immersed in PBS are given. In cross comparisons with an IR camera, the measurements validate the superiority of the Raman approach in the noninvasive characterization of temperature at a microscopic scale.

Methods

Microscopic Raman Spectroscopy

The setup that was used to excite and record the spectrum is based on a Nikon Diaphot inverted microscope with standard 4, 10, and 20 \times objectives (Figure 1). The Diaphot model is particularly flexible as it has a very open area above the stage with a retractable illuminator, two output ports plus the binocular eyepieces, an under the turret rear illumination path typically used for epifluorescence, and a dichroic filter bay, which accepts standard cube filter holders. The rear illumination periscope tube was stripped of its collimating lenses, the front left optical port was fitted with an inexpensive cooled charge-coupled device (CCD) camera (model 3.3MPC), and the front 35-mm camera port was used to interface to a standard focusing objective (20 \times) and a multimode optical fiber (diameter, 50 μm). The rear illumination lamp tube was removed, and the port was fitted with a 671-nm clean up filter (660–680 nm). A free-space DPSS 671-nm, 200-mW diode laser (model VA-I-N-671) was optically guided by a folding mirror into the rear illumination tube in which the nearly collimated beam passes

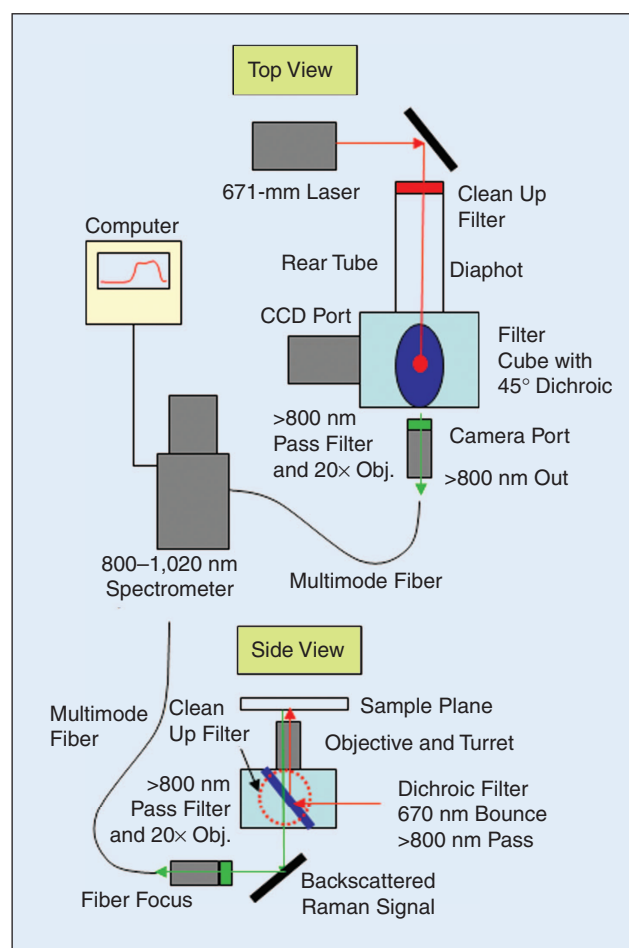


Fig. 1. Block diagram of the Diaphot microscope setup and optical paths.

A small fan was used to speed up the cooling by increasing air convection.

laterally into the filter cube and then bounces upward by a 45° flat made up of a 700-nm-long wavelength-pass dichroic filter (High Efficiency Cold Mirror). The laser light is then routed through the objective turret and focused onto the plane of the sample stage. The laser was set at a constant current of 2.0 A, yielding 300 mW of power at the laser output, which was reduced to approximately 70 mW at the sample plane after passing through the folding mirror, cleanup filter, turret glass, dichroic cube filter, and $20\times$ objective lens.

The backscattered Raman light was captured, collimated by a $20\times$ objective, filtered from the backscattered Rayleigh light by the dichroic mirror in the filter cube, and, following the microscope optical path, directed forward to the 35-mm camera port where it was apertured by the film cutout built into the microscope. The beam was then passed through a long wavelength-pass filter (>785 nm, BLP01-785R-25) to further block the backscattered Rayleigh light and any stray laser light from the sample that passed through the dichroic mirror. Finally, the beam was refocused by a $20\times$ objective onto a multimode fiber with a standard subminiature version A (SMA) connector. The fiber was centered on the beam using a fiber launch positioning jig (model MBT612). The fiber was coupled into a spectrometer (Shamrock SR-163) with cooled electron-multiplying CCD (iDUS DV420A) through a standard fiber line collimator and no additional coupling slit. A photo of the entire system is shown in Figure 2.

To assure that the laser pump and optical path to the spectrometer and CCD ports overlapped exactly, the pump

laser focal spot was coaligned with the top illuminator by adjustments to the laser position and angle and the collinear red and white spots verified in the CCD camera (Figure 3). The laser spot diameter determines the primary area sampled in the spectrometer as all the backscattered energy from this region was collected and focused onto the optical fiber by the second $20\times$ objective at the camera port. The spectrometer was used to peak up the Raman signal from the water sample through adjustments of the objective-to-fiber coupling stage, as well as optimization of the position of the objective within the slightly larger camera port aperture.

Using the aforementioned filters and the Andor SR-163 spectrometer with 300 lines/mm grating, the transmitted range of backscattered Raman light was between 800 and 1,020 nm with 0.8-nm resolution. Employing the 671-nm laser pump, the $3,200\text{--}3,500\text{ cm}^{-1}$ vibrational water peaks appear between 855 and 880 nm. An added bonus is the presence of two strong and relatively narrow Raman shifted peaks of polystyrene at approximately $3,140\text{ cm}^{-1}$ that appear at 850 nm and were present in the Corning and Falcon plastic petri dishes as well as in an enclosed thickness-controlled and gas-permeable cell culture dish (Nunc OptiCell Culture System) but not in a glass slide, glass cover slip, or quartz glass (Figure 4). The polystyrene peak fell directly outside the water spectrum and can be used to determine the axial focal plane of the pump laser. This line appears as the focal plane of the objective passes through the plastic. An additional benefit of the OptiCell dish is having both a top and bottom plastic membrane (spaced 2 mm apart),

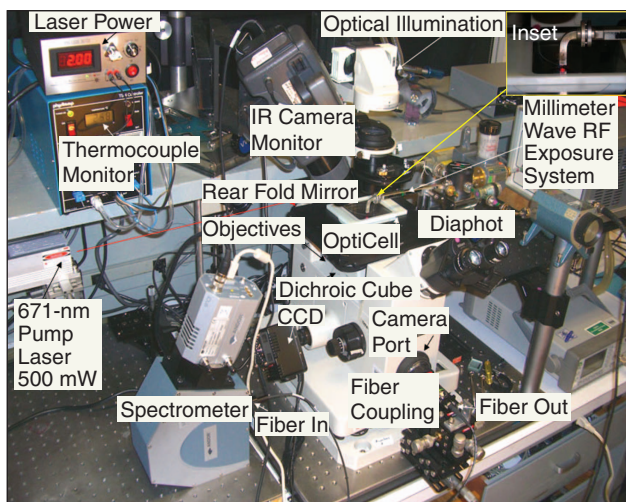


Fig. 2. Photo of instrument setup showing pump laser, IR monitor camera, thermocouple monitor, OptiCell culture dish, camera port fiber coupler, spectrometer, and millimeter wave exposure system with the waveguide output on top of the biosample.

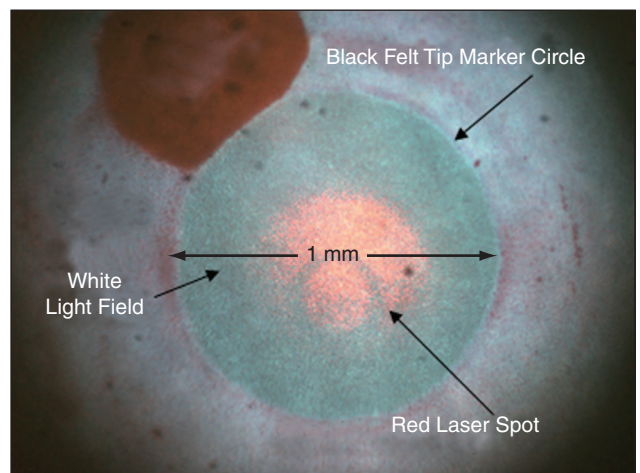


Fig. 3. CCD picture through eyepiece showing coaligned 671-nm laser light spot and top white-light illumination spot on a 1-mm diameter circle drawn on a piece of ground glass positioned at the objective focus. The dark rim around the edge of the field is the out of focus aperture of the white-light illuminator used to center the illuminator over the field of view.

which demarcates a scan through the internal liquid sample by the appearance, disappearance, and reappearance of the polystyrene Raman peaks (Figure 5).

The appearance of the two polystyrene peaks at 850 nm was evident even at 0.5-s-long integration time in the spectrometer and could be used to quickly calibrate the focus wheel of the microscope as well as peaking up the overall signal. Depending

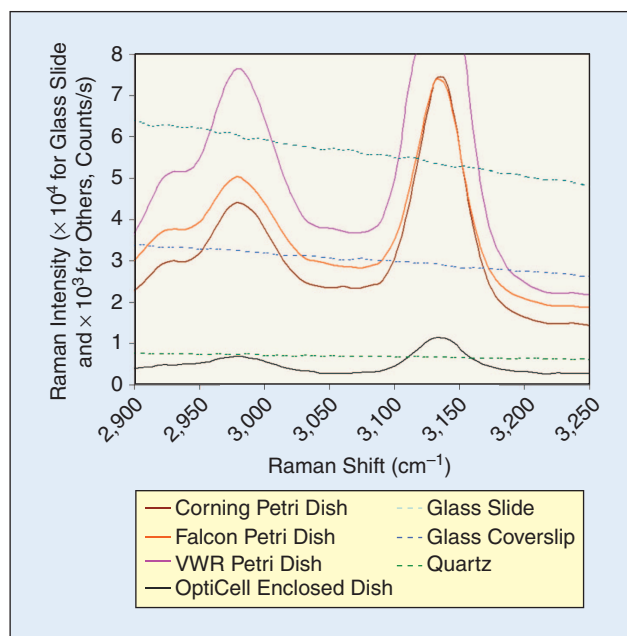


Fig. 4. Raman spectra of polystyrene-based culture dishes, glass, and quartz. The 850-nm peak is present in Corning (430166), Falcon (25369-022), and VWR (25384-302) petri dishes as well as in OptiCell dishes. Glass samples, such as a 1-mm-thick glass slide (48300-025, VWR) and 0.15- μ m-thick cover slip (48366-067, VWR) were highly fluorescent, while a 1-mm-thick quartz glass was remarkably opaque.

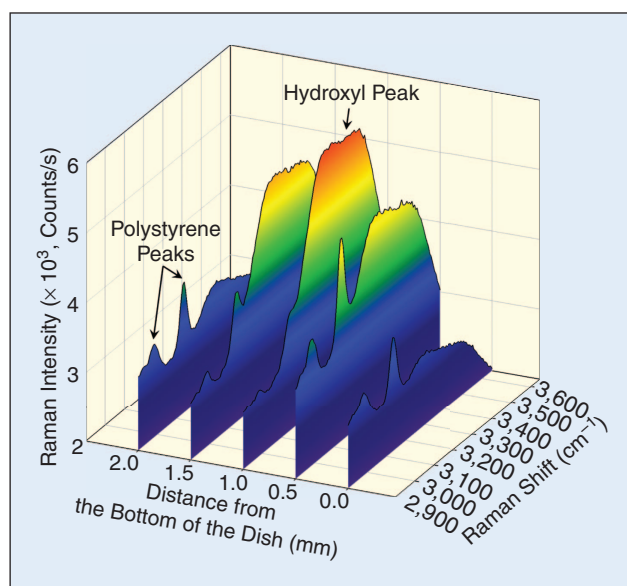


Fig. 5. Raman spectra showing progression of focal plane from the bottom, through 2 mm of water, and to the top of an OptiCell dish.

on the location of the attached cells at the top or bottom membrane of the OptiCell dish, the focal plane of the microscope could then be precisely adjusted for measuring the Raman signal from the cells rather than the adjacent medium. The integration time of the spectrometer was then set to 8 s per measurement to improve the signal-to-noise ratio of the collected data.

Temperature Measurement and Controlled General Heating

The configuration, depicted in Figure 6, was employed to measure the Raman spectra in the 800–1,020 nm range of various samples of deionized (DI) water and water-based culture media as a function of temperature. In each case, 10 mL of solution was injected into an OptiCell dish, and all air bubbles were removed to leave a uniform 2-mm-thick fluid sample sandwiched between the 75- μ m-thick treated polystyrene membranes. To accurately measure the temperature of the fluid in the region directly around the illuminated sample, two separate independent monitors were set up. A noncontact thermal IR imaging camera with 0.1 $^{\circ}$ C discrimination (Infra-metrics Thermacam PM290) was positioned above the sample stage and it continually recorded the sample temperature over an approximate area of 1.5×1.5 cm^2 at a resolution of approximately 50×50 μm^2 . This camera allowed us to monitor the uniformity of the temperature changes over a wide region around the sample. As an absolute monitor of the fluid temperature inside the OptiCell and directly adjacent to the field of view, a miniature coaxial type T thermocouple probe with 0.6 mm-diameter sampling tip, 0.1-s time constant, and 0.1 $^{\circ}$ C accuracy (IT-18, Physitemp) was inserted into the OptiCell holder through a 22-gauge needle and positioned immediately outside the viewing circle of the 20 \times microscope objective (marked on the plastic with a felt tip pen) (Figure 7). The OptiCell dish with the inserted thermocouple was air sealed using a small dab of polydent around the needle entry point, bridging the thermocouple wires but allowing easy removal for later use. Between the thermocouple and IR

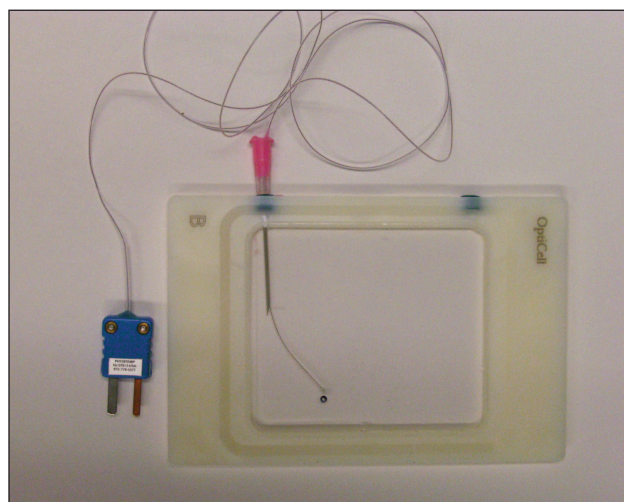


Fig. 6. Photo of the OptiCell dish filled with DI water with the inserted coaxial thermocouple probe sitting next to the area to be illuminated and spectrally imaged (black circle, 1 mm in diameter). The clear area is 75 \times 65 mm. The fluid thickness is 2 mm, and the top and bottom polystyrene films are 75- μ m thick.

The RF power and absolute frequency from the millimeter wave generator were measured directly using calibrated detectors.

camera, the region being directly illuminated by the pump laser and imaged through the CCD and camera (spectrometer) ports could be continuously monitored.

Because of the small volume (10 mL) and large area (50 cm²) of the OptiCell dish, it was extremely simple to slowly heat (or cool) the entire sample with a small hair dryer and fan. During data collection, the hair dryer was used to flow warm air across the surface of the cell, and the IR camera was used to make sure the area around the sample spot stayed at a uniform temperature while the thermocouple measured the absolute temperature of the fluid itself, just outside of the laser illumination circle. The measurements were then repeated during a cooling cycle. For the temperatures approaching ambient, a small fan was used to speed up the cooling by increasing air convection. During all temperature manipulations (both heating and cooling), the temperature change was considerably slower (0.5 °C/min) than the integration time of the spectrometer (8 s).

Focal Heating Using RF Millimeter Wave Exposure System

One practical use of the remote focal thermal monitoring in our laboratory was related to monitoring temperature changes in cell cultures during exposure to high-frequency RF radiation (millimeter and submillimeter waves, frequencies between 60 and 600 GHz). As the application of these relatively untapped spectral bands expands into the areas of communications, imaging, and security, there is a growing need to understand what, if any, impact this penetrating radiation has on cellular processes. One measure of such impact is the change in temperature induced in cell cultures and tissues. Measuring such changes during and after RF exposure at a microscopic level is extremely difficult. As mentioned earlier, thermal IR cameras and microscopes tend to measure only the surface temperature, especially in water-based media. If the cells reside at the bottom of a media container, it may be impossible to accurately record any temperature rise on this layer using standard IR techniques. The Raman scattering measurements described in this article allow one to position the axial focal spot at any point within the (relatively small) volume of the culture dish. It makes it simple with such a system to illuminate the cells with RF energy from the top (Figure 2, center) while monitoring the temperature and any visible changes in the cells via the bottom, using the normal viewport of an inverted microscope.

The setup for RF exposure is shown in Figure 2, with a close up of the microscope stage area in the inset. A millimeter wave generator consisting of a commercial 50–75 GHz swept frequency backward wave oscillator (BWO, formerly Micronow model 705 sweeper with a Siemens RWO-50 tube) was used to inject RF power through a series of waveguide components that terminate and hence radiate directly onto the top of the OptiCell polystyrene membrane. The polystyrene has very low RF loss,

and the WR-15 waveguide (1.9 × 3.8 mm² aperture) is loaded with a tapered PTFE wedge to match the power into the plastic with only minor reflections. The cells were adhered to the top of the container and thus were directly impacted by the RF energy before it could be absorbed by surrounding culture medium. The RF power and absolute frequency from the millimeter wave generator were measured directly using calibrated detectors that are switched into the RF path and the power incident on the OptiCell is inferred by measuring the losses through the extra waveguide between the switch and sample. An in-line calibrated attenuator is used to vary the incident power in known steps.

Measurements consisted of placing a large-cell cluster directly under the RF waveguide and applying fixed frequency (60 GHz) calibrated RF power to the OptiCell for a fixed period of time (approximately 4 min) until the temperature rise in the surrounding medium reached an equilibrium, as measured by the IR camera. The highest power level was applied first, and the cells were allowed to cool for several minutes before the next exposure. The IR camera cannot view and measure the temperature directly under the waveguide, where the power output is peaked, because the metal guide hides this region from a top view. The camera can only record the temperature directly surrounding the metal waveguide aperture (approximately 2 mm from the center illumination hot spot). However, the Raman signal is collected from below and is easily tagged directly to the center of the cell field. The RF output from the waveguide aperture roughly follows a Gaussian power distribution, which rolls off from the center of the field in an approximately spherical pattern. Little or no

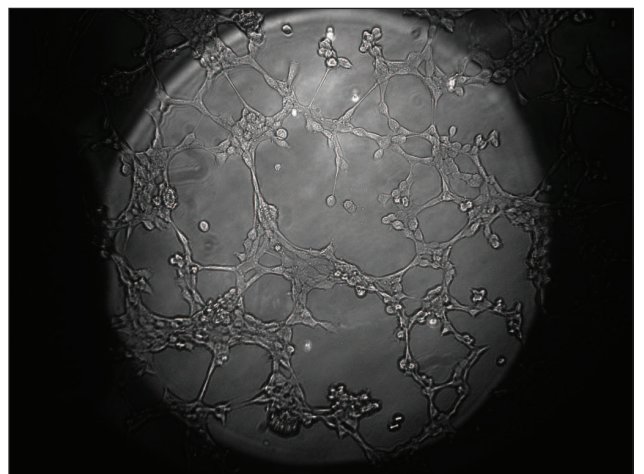


Fig. 7. Microphotograph of H1299 cells adhered to the OptiCell membrane, taken through the CCD camera port with a 20× objective. The black circle (1 mm in diameter) is marked on the membrane for subsequent localization of the cells for time-lapse imaging.

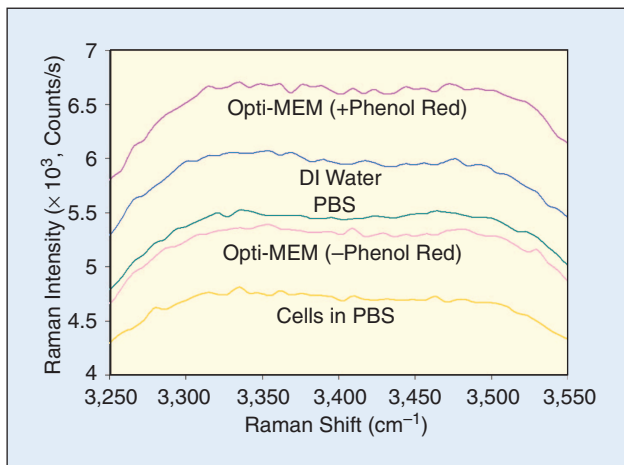


Fig. 8. Raman spectra of various water-based media inside the OptiCell dish at 25°C. Although changes in total signal are apparent because of the amount of Raman backscatter, the spectral line shape is very consistent.

power penetrates through to the bottom of the OptiCell as the PBS is extremely absorbing at this frequency.

The cell culture was exposed to three levels of RF power (approximately 3.6, 7.2, and 14.4 mW at the waveguide output port), which varies little over the field of view (approximately 1 mm²) produced by the 20× objective. This power is spread over an area of approximately 2.8 mm² (set by the waveguide aperture and frequency) giving a maximum power density of approximately 5.2 mW/mm² for the exposure at 14.4 mW. Note that this power level is much greater than the suggested safe limit for the long-term human exposure of 0.1 mW/mm². The Raman spectra were recorded as the temperature was measured by the IR camera in the region directly outside the waveguide aperture. Several cell locations were examined in

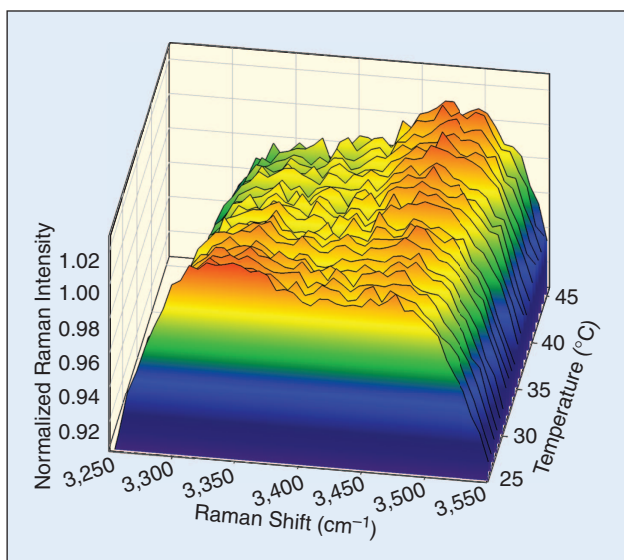


Fig. 9. Temperature dependence of Raman spectrum in DI water between 25.2 and 44.2°C at 1°C intervals. All data are collected from the same position on the OptiCell dish and referenced against the in situ thermocouple. The pump laser was focused approximately in the middle of the 2-mm-thick sample.

the culture dish (OptiCell), making it impractical to include a separate microthermocouple probe near each exposure area.

Cell Culture

The H1299 immortalized epithelial cell line is derived from human lung carcinoma and was a gift from Dr. Alex Sigal. This cell line is characterized by rather large cells that strongly adhere to all tested plastic surfaces, including those of the petri dishes and of the OptiCell thin-membrane dish and is the major reason for choosing this particular line for our early investigations (Figure 7). The cells were grown in RPMI-1640 medium, supplemented with 10% (v/v) fetal bovine serum and 2 mM L-glutamine, in a 5% CO₂ incubator set at a 37°C. For spectroscopy measurements, RPMI was replaced with PBS (pH 7.4). As a possible substitution for PBS, we also evaluated Opti-MEM, as it exhibits the best optical transparency among the phenol-red-containing media. Opti-MEM is a modification of Eagle's minimal essential medium with a reduced amount of phenol red (1.1 mg/L) when compared with the standard Dulbecco's modified eagle's medium (15 mg/L).

Results

Raman Hydroxyl Band in Different Culture Media

Measurements of the Raman spectrum were made in DI water, PBS, Opti-MEM with and without phenol red, and a confluent layer of cells in PBS. In all cases, a 20× objective was used. The focal spot being sampled by the Raman spectrometer was approximately 1 mm in diameter. The laser power was 70 mW, and the spectrometer integration time was 8 s. A background count with the laser off was used for subtraction of the CCD dark current and read-out noise. A typical set of spectra are shown in Figure 8 at a single temperature (25°C). The amplitude of the Raman hydroxyl band varied among the media tested, with the highest intensity seen in the Opti-MEM medium with phenol red. The amplitude of the Raman hydroxyl band signal was lower in cells than in water or water-based media, in concordance with another study [18]. No discernable difference was observed in the shape of the hydroxyl band among the various media, DI water, and cells. Because of their lower background intensities when compared with the phenol-red-containing culture medium, we selected the DI water and PBS for the subsequent heating studies.

Analysis of the Shape of the Raman Hydroxyl Band in Water and Cells During Uniform Heating

The Raman signal at the hydroxyl band was collected at gradually increasing and decreasing temperatures in the physiological range of 25–45°C as measured by the thermocouple. The changes in the shape of the Raman hydroxyl band were remarkably similar for the DI water (Figure 9) and cells in PBS (Figure 10). In addition to point-sampling of the temperature inside the OptiCell dish, spatial distribution of the temperature was assessed by an IR camera. It showed a uniform temperature (within 0.2°C) on top of the OptiCell dish over a large area surrounding the illumination circle. However, the absolute temperature values, measured by the IR camera, varied by as much as 0.8°C when compared with the thermocouple readings. For this reason, only the thermocouple readings were used for correlation with the Raman changes in this study.

Before the peak-fitting analysis, the Raman spectrum data were normalized based on the isosbestic point of the Raman

hydroxyl band found to be at $3,440\text{ cm}^{-1}$. The isosbestic point refers to the wavenumber at which spectra taken at different conditions (e.g., temperatures, pressures, and potentials) cross putatively due to the equilibrium between the hydrogen-bonded and nonhydrogen-bonded hydroxyl species [19], [20]. The isosbestic point value in this study is well within the determined $3,400\text{--}3,500\text{ cm}^{-1}$ range for the liquid water under different polarization conditions [9], [19].

For the analysis of the shape of Raman hydroxyl band, we decided to apply an automated double-peak fitting procedure that does not impose any a priori restrictions on the shape or location of the peaks. We used the Fityk program (<http://www.unipress.waw.pl/fityk/>), which included three options for automated nonlinear optimization of the double-peak fitting: Levenberg-Marquardt, Nelder-Mead simplex, and the genetic algorithm. Of these, Levenberg-Marquardt produced the most consistent results due to avoidance of local minima. We have evaluated several peak functions, including the Gaussian, Lorentzian, Pearson VII, and approximated Voigt/Faddeeva (a convolution of Gaussian and Lorentzian functions). Of these, the approximated Voigt/Faddeeva function [21] proved to be the most robust. On the basis of initial evaluation, we decided to use the Levenberg-Marquardt optimization method and the approximated Voigt/Faddeeva function for the automated double-peak fitting in this study.

Peak fitting was initially performed for the water Raman spectrum at the 25.2°C nominal temperature (Figure 11). To facilitate the comparison between the peaks, we chose the option for fitting both peaks with functions of the same shape, but let the program to choose the actual optimal shape. In the subsequent peak fittings for the water and cellular spectra at higher temperatures, we kept the wavenumber values of both peaks ($3,289$ and $3,518\text{ cm}^{-1}$) and the shapes of the peaks (-21.32) constant, so that the only variables in the peak fitting were the height and width of the peaks. Area under the peaks was a product of these variables. The ratio of areas under peak 2 versus peak 1 indicated

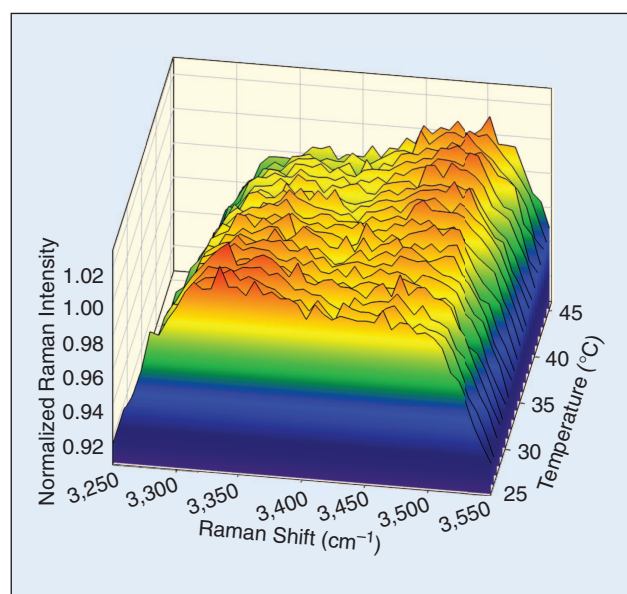


Fig. 10. Temperature dependence of Raman spectrum in H1299 immortalized epithelial cell line between 25.2 and 44.2°C at 1°C intervals. The cells were cultured in RPMI medium in OptiCell dish at 37°C and $5\%\text{ CO}_2$. For spectroscopy measurement, the RPMI was replaced with PBS.

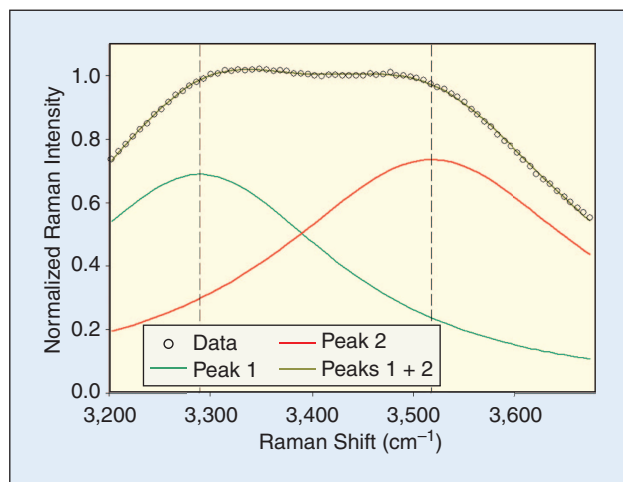


Fig. 11. Double-peak fitting of the OH stretching band at a temperature of 25.2°C on a 2-mm-thick sample of DI water in an OptiCell dish. The peak functions are the approximated Voigt/Faddeeva (a convolution of Gaussian and Lorentzian functions). Both peaks were specified to have the same shape, allowing the common shape and individual center wavenumbers, heights, and widths of the peaks to be varied using an automated Levenberg-Marquardt optimization method for double-peak fitting. For the subsequent peak fittings at higher temperatures, the shape of the peaks and the peak-center wavenumbers were kept constant.

the temperature-dependant expansion of peak 2 relative to peak 1 (Figure 12). Linear regression analysis showed that the ratio of the two spectral peak regions provides an accuracy of at least 1°C . Higher accuracy would be possible with a more sensitive spectrometer. Peak 2/1 area ratio for the cells was significant larger than that for the DI water, as calculated by a paired *t*-test

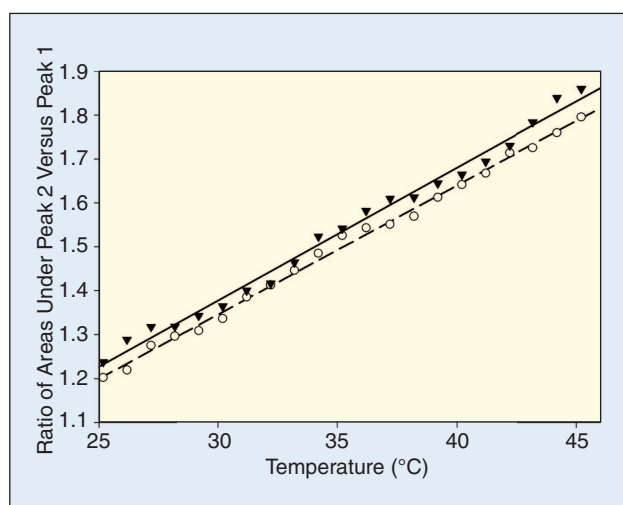


Fig. 12. Ratio of the areas under peak 2 versus peak 1 of the OH stretching Raman band at temperatures between 25.2 and 44.2°C of DI water (outlined circles) and H1299 cells in PBS (solid triangles) in an OptiCell dish. Linear regression for the DI water data ($R^2 = 0.996$) is shown as a dotted line and for the H1299 cells ($R^2 = 0.990$) as a solid line. Inset shows a close-up view of the OptiCell dish with the laser light coming in from below and millimeter wave waveguide aperture above.

($p < 0.001$), while the slope of both regression lines was practically identical (0.0294 for water and 0.0303 for cells).

Analysis of the Shape of the Raman Hydroxyl Band in Water and Cells During RF Heating with Millimeter Waves

In this experiment, the cells in PBS were locally heated by RF millimeter wave energy using a metal waveguide matched to, and directly in contact with, the upper polystyrene membrane of the OptiCell. The thermocouple probe could not be used in this setup, as it could not be easily positioned within the OptiCell and would perturb the cell attachment. It is also likely that the readings of the thermocouple would have been affected by direct coupling of the RF radiation to the metal sensing element (although this was not tested explicitly). Therefore, before the millimeter wave exposure, a baseline reading of the uniform temperature at the top OptiCell surface was taken by the IR camera while the waveguide was lifted off the surface. During RF exposure, the IR camera could no longer read the temperature directly from the irradiated area as it was shadowed by the waveguide aperture (see Figure 2 inset). Readings were instead taken at the hottest spot immediately adjacent to the waveguide. These IR camera readings, which were expected to be somewhat lower than the temperature directly under the exposure port, were compared with remote temperature measurements obtained by our microscopic Raman spectroscopy technique. Calibration of the Raman readings to an absolute temperature value was done by correlating the baseline IR camera reading with the Raman peak 2/1 area ratio with no RF present. The temperature values during exposure to three levels of millimeter waves (3.6, 7.2, and 14.4 mW) were calculated

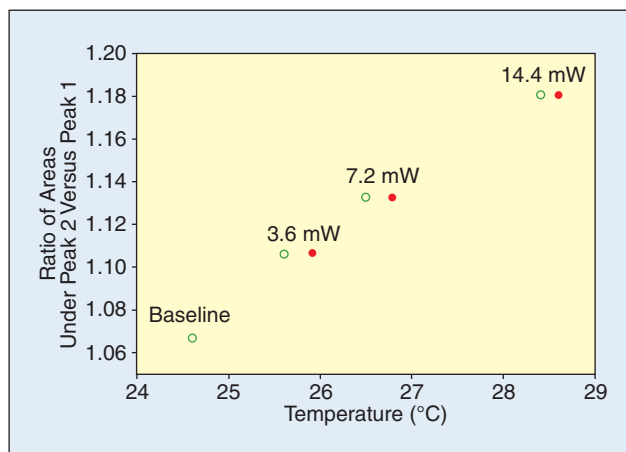


Fig. 13. Ratio of the areas under peak 2 versus peak 1 of the OH stretching Raman band during RF heating with three levels of millimeter wave power (3.6, 7.2, and 14.4 mW) introduced via a matched WR-15 waveguide aperture (1.88×3.76 mm). The green circles indicate the temperature measurements immediately adjacent to the waveguide, but well outside the field of view, taken with the IR camera, while the red circles indicate the calculated temperature values directly under the center of the waveguide and not visible in the camera. The calculated points are derived from the baseline IR camera reading (no waveguide present) and the slope of 0.03 measured with the thermocouple and heater on an identically configured OptiCell. At the baseline reading, the white and black circles are overlapped.

using the slope value of 0.03 obtained in the earlier calibration experiment with PBS (Figure 13, black dots). Between each millimeter wave exposure, the cells in the OptiCell dish were cooled until they reached the baseline temperature, as measured by the IR camera. The Raman-based temperature readings during the exposure were consistently higher than the IR camera readings (Figure 13, white dots), confirming our ability to measure actual focal plane heating without direct visual or thermocouple access in a microscopic region. The considerable millimeter wave-induced heating (approximately 4°C), observed in the cells during the RF exposure at 14.4 mW, can be contrasted with a lack of any detectable heating in the cells during exposure to 70 mW of laser light at 671 nm as measured by the thermocouple. This highlights the dramatic difference in absorption by water at the two wavelengths.

Discussion

The present study describes the setup and use of a simple, low-cost, flexible Raman spectrometer system for remote measurement of the temperature in water-based media on a microscopic scale. The absolute temperature can be inferred from a ratiometric evaluation of dual peaks in the Raman hydroxyl band at the $3,200\text{--}3,700\text{ cm}^{-1}$. The measured Raman spectrum falls into the region of $800\text{--}900\text{ nm}$, permitting the use of standard microscope objectives and optical filters, a low-cost optical pump laser, and a convenient fiber-coupled spectrometer with a standard CCD, not optimized for the near-IR. The most expensive part of the measurement system is the spectrometer which costs between US\$10,000 and US\$15,000. The microscope, laser, filters, and fibers were obtained for under US\$10,000 total. The use of the $800\text{--}900\text{ nm}$ band significantly reduces the background noise from fluorescence inherent to biological samples. The described setup has been used to measure the temperature dependence of DI water and cells in PBS. Temperature accuracy of 1°C has been attained with 8-s sampling by employing an automated nonlinear optimization method for double-peak fitting in the Raman hydroxyl band. The technique should prove useful for monitoring temperature changes in culture media without the need for direct thermocouple probing and through common culture plates composed of polystyrene or quartz. The use of plastic dishes provides the added advantage of being able to visualize a narrow spectral signature from polystyrene near the hydroxyl stretching band (at 850 nm) that can be used to accurately [within the numerical aperture (NA) of the objective] determine the axial focal plane in the culture dish. The strength of the Raman polystyrene signal allows short measurement times (less than 1 s) for fast and precise focusing and alignment of the spectroscopic optical elements. Phenol-red-containing medium should be avoided during the spectrometric temperature measurements because of its high fluorescence background, reducing the signal-to-noise ratio at the Raman hydroxyl band. However, minimal background fluorescence was observed in phenol-red-free culture medium and PBS.

The instrument was used to record, for the first time, the direct rise in temperature of a cluster of cells adhered to a polystyrene membrane and immersed in PBS, under direct exposure to millimeter wave radiation. The technique successfully recorded a significant temperature difference in the region directly under the RF beam from that of the nearest accessible region (viewed by an IR camera), which lay directly outside the exposure area. In addition, by calibrating the axial focal spot of the objective lens with the Raman peaks,

it was possible to measure the temperature at the plane of the cells and through 2 mm of PBS solution. We believe these are the very first measurements of this type and lay the groundwork for much more extensive investigations of the impact of RF radiation on cells and cell processes.

In a similar fashion, this setup can be used to monitor thermal changes on the micron scale associated with local application of drugs, affecting thermoplastic cellular functions (e.g., metabolism).

In summary, we have described a simple inexpensive method for quick, precise, and reliable remote microscopic measurement of cellular temperature inside the culture medium, which is applicable to a wide range of problems in microthermometry of biological systems.

Acknowledgments

The authors gratefully acknowledge the contributions of Ms. Kathleen Teves, a summer undergraduate research assistant from the University of California (UC) Irvine, for collecting the measurements data and the continuing support of Caltech Profs. David B. Rutledge and Scott E. Fraser. They also thank Dr. Alex Sigel for the H1299 cell line, and they especially thank Mr. Jay Moskovic for the loan of the Andor spectrometer. This work was carried out under grants from the National Institutes of Health.



Victor Pikov received his Ph.D. degree in cell biology from Georgetown University, where he evaluated plasticity in micturition-related reflexive circuitry after spinal cord injury. During postdoctoral fellowship at the California Institute of Technology, he expressed an optically activated ion channel in virally transected neurons.

He is currently a neural engineer/neurophysiologist at the Neural Engineering Program of the Huntington Medical Research Institutes (HMRI). He also works as a director of the Summer Undergraduate Research Program at HMRI. His research interests include three main areas of neural engineering: development and in vivo testing of intelligent bidirectional arrays of silicon-based multisite probes for studying and controlling neuronal function; applying these multisite probes for monitoring and modulating changes in spinal, pontine, and cortical neuronal excitability in animal models of spinal cord injury, tinnitus, stroke, and migraine; and noninvasive neuronal stimulation using millimeter waves.



Peter H. Siegel received his B.A. degree in astronomy from Colgate University in 1976, M.S. degree in physics from Columbia University in 1978, and his Ph.D. degree in electrical engineering from Columbia University in 1983. He has been involved in terahertz (THz) technology and applications for more than 30 years. He

worked as a Columbia Radiation Laboratory and Nuclear Regulatory Commission (NRC) fellow at the National Aeronautics and Space Administration (NASA) Goddard Institute for Space Studies in New York and on the staff of the National Radio Astronomy Observatory in Charlottesville, Virginia. He joined the Jet Propulsion Laboratory in 1987 where he formed and currently leads the Submillimeter Wave Advanced

Technology (SWAT) team, a group of 25 engineers working on the development of submillimeter-wave technology for NASA's near- and long-term space astrophysics, earth remote sensing, and planetary mission applications. He maintains joint appointments at Caltech in both biology and electrical engineering where he is focused on THz biomedical applications. He has served as cochair and chair of IEEE Microwave Theory and Techniques (MTT) Committee 4-THz Technology and as an IEEE distinguished microwave lecturer. He is currently chair of the International Society of Infrared, Millimeter, and Terahertz Waves, the oldest and largest conference venue devoted to THz technology and applications.

Address for Correspondence: Peter H. Siegel, Beckman Institute, MC 139-74, California Institute of Technology, 1200 E. California Blvd., Pasadena, CA 91125, USA. E-mail: phs@caltech.edu.

References

- [1] P. B. Roush, Ed., *The Design, Sample Handling, and Applications of Infrared Microscopes*. West Conshohocken, PA: ASTM, 1987.
- [2] N. Kakuta, F. Li, and Y. Yamada, "A method for measurement of water temperature in micro-region using near infrared light," in *Proc. 27th Ann. Int. Conf. Engineering in Medicine and Biology Society*, 2005, pp. 3145–3148.
- [3] N. Kakuta, H. Arimoto, H. Momoki, F. Li, and Y. Yamada, "Temperature measurements of turbid aqueous solutions using near-infrared spectroscopy," *Appl. Opt.*, vol. 47, pp. 2227–2233, 2008.
- [4] V. S. Hollis, T. Binzoni, and D. T. Delpy, "Noninvasive monitoring of brain tissue temperature by near-infrared spectroscopy," in *Optical Tomography and Spectroscopy of Tissue IV (Proc. SPIE)*, B. Chance, R. R. Alfano, B. J. Tromberg, M. Tamura, and E. M. Sevick-Muraca, Eds., 2001, pp. 470–481.
- [5] J. J. Kelly, K. A. Kelly, and C. H. Barlow, "Tissue temperature by near-infrared spectroscopy," in *Optical Tomography, Photon Migration, and Spectroscopy of Tissue and Model Media: Theory, Human Studies, and Instrumentation (Proc. SPIE)*, 1995, pp. 818–828.
- [6] S. A. Rice, "Conjectures on the structure of amorphous solid and liquid water," *Top. Curr. Chem.*, pp. 109–200, 1975.
- [7] E. Libowitzky, "Correlation of O-H stretching frequencies and O-H center dot center dot center dot O hydrogen bond lengths in minerals," *Monatsh. Chem.*, vol. 130, pp. 1047–1059, 1999.
- [8] D. Simonelli and M. J. Shultz, "Temperature dependence for the relative raman cross section of the ammonia/water complex," *J. Mol. Spectrosc.*, vol. 205, pp. 221–226, 2001.
- [9] G. E. Walrafen, M. R. Fisher, M. S. Hokmabadi, and W. H. Yang, "Temperature dependence of the low- and high-frequency Raman scattering from liquid water," *J. Chem. Phys.*, vol. 85, pp. 6970–6982, 1986.
- [10] J. L. Green, A. R. Lacey, and M. G. Sceats, "Spectroscopic evidence for spatial correlations of hydrogen bonds in liquid water," *J. Phys. Chem.*, vol. 90, pp. 3958–3964, 1986.
- [11] S. M. Pershin, A. F. Bunkin, V. A. Lukyanenko, and R. R. Nigmatullin, "Detection of the OH band fine structure in liquid water by means of new treatment procedure based on the statistics of the fractional moments," *Laser Phys. Lett.*, vol. 4, pp. 809–813, 2007.
- [12] H. D. Lutz, "Structure and strength of hydrogen bonds in inorganic solids," *J. Mol. Struct.*, vol. 646, pp. 227–236, 2003.
- [13] D. Risovic and K. Furic, "Comparison of Raman spectroscopic methods for the determination of supercooled and liquid water temperature," *J. Raman Spectrosc.*, vol. 36, pp. 771–776, 2005.
- [14] J. B. Brubach, A. Mermet, A. Filabozzi, A. Gerschel, and P. Roy, "Signatures of the hydrogen bonding in the infrared bands of water," *J. Chem. Phys.*, vol. 122, p. 184509, 2005.
- [15] G. E. Walrafen, W. H. Yang, Y. C. Chu, and M. S. Hokmabadi, "Raman OD-stretching overtone spectra from liquid D₂O between 22 and 152°C," *J. Phys. Chem.*, vol. 100, pp. 1381–1391, 1996.
- [16] D. M. Carey and G. M. Korenowski, "Measurement of the Raman spectrum of liquid water," *J. Chem. Phys.*, vol. 108, pp. 2669–2675, 1998.
- [17] J. D. Smith, C. D. Cappa, K. R. Wilson, R. C. Cohen, P. L. Geissler, and R. J. Saykally, "Unified description of temperature-dependent hydrogen-bond rearrangements in liquid water," *Proc. Natl. Acad. Sci. U. S. A.*, vol. 102, pp. 14171–14174, 2005.
- [18] S. A. Thompson, F. J. Andrade, and F. A. Inon, "Light emission diode water thermometer: A low-cost and noninvasive strategy for monitoring temperature in aqueous solutions," *Appl. Spectrosc.*, vol. 58, pp. 344–348, 2004.
- [19] G. E. Walrafen, M. S. Hokmabadi, and W. H. Yang, "Raman isosbestic points from liquid water," *J. Chem. Phys.*, vol. 85, pp. 6964–6969, 1986.
- [20] P. L. Geissler, "Temperature dependence of inhomogeneous broadening: On the meaning of isosbestic points," *J. Amer. Chem. Soc.*, vol. 127, pp. 14930–14935, 2005.
- [21] R. J. Wells, "Rapid approximation to the Voigt/Faddeeva function and its derivatives," *J. Quant. Spect. Radiat. Trans.*, vol. 62, pp. 29–48, 1999.